MATERIALS CHEMISTRY
FRONTIERS

Accepted Manuscript

This article can be cited before page numbers have been issued, to do this please use: D. Patra and A. Ajayaghosh, *Mater. Chem. Front.*, 2026, DOI: 10.1039/D6QM00340K.

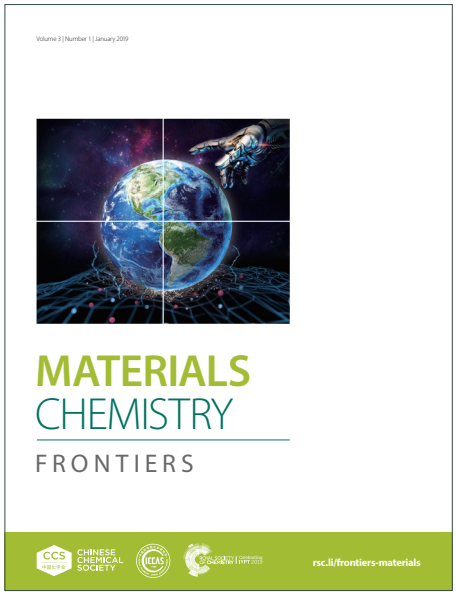

View Article Online
DOI: 10.1039/D6QM00340K

ARTICLE

Customization of Cloud Temperature in Amphiphilic π-Systems by Photoisomerization and Supramolecular Co-assembly for Smart Window Application

Received 00th January 20xx,
Accepted 00th January 20xx

DOI: 10.1039/x0xx00000x

Dipak Patra[a,b] and Ayyappanpillai Ajayaghosh* [a,b,c]

Controlling the phase transition temperature of amphiphilic polymers and small molecular systems exhibiting Lower Critical Solution Temperature (LCST) phenomenon is crucial to regulate the transmittance of light, required for the construction of thermoresponsive smart windows. To address this problem, we have taken advantage of photoisomerization and supramolecular co-assembly of two photoresponsive amphiphilic molecules, an anthracene-derived cyanostilbene (**ANT**) and a pyrene-derived cyanostilbene (**PYR**), exhibiting different LCST phase transitions at 27 and 37 °C, respectively. Initially, aqueous solutions (1 mM) of these molecules, when heated above their LCST under ambient light, exhibited a 90% reduction in solar light transmittance owing to the increase in particle size from 10-20 nm to 0.6-1.3 μm. Subsequently, the phase transition cloud temperatures (T_{cloud}) could be customized by photoisomerization and co-assembly of the two molecules at different mole ratios. This approach allowed control of the particles size between 675-1300 nm during the LCST phase change, enabling the fine-tuning of T_{cloud} between 27-37 °C. Smart windows fabricated with **ANT** and **PYR** and their 1:1 combination exhibited solar and luminous transmittance reduction from 81% and 84% to 1.7% and 1.6% respectively, at 27 °C. Thermal IR transmittance was drastically reduced from 78% to 1.8%. This approach has been used to design several custom-made smart window prototypes with controlled transparency modulation suitable for tropical climates.

Introduction

Lower Critical Solution Temperature (LCST) is an entropy-driven phase change from fibrillar to globular structures exhibited by certain amphiphilic polymers such as polyacrylamide in water medium.[1-4] These materials undergo phase transition from transparent-to-opaque states and vice versa in response to external temperature, thus regulating the transmittance of heat-generating IR radiation by facilitating the scattering of solar radiation.[5-8] Hence, they are used for the construction of thermoresponsive smart windows.[9-11] When compared to the photo- and electrochromic smart windows, thermoresponsive polymer-based windows exhibit remarkable advantages of passive control of sunlight with zero energy input and hence are relatively cheap, easy to construct and operate.[12-18] However, polymers have several disadvantages, such as inconsistency in the molecular weight with batchwise synthesis and the associated variations in the particle size formation which adversely impact on the scattering efficiency required for the filtering of the heat generating IR radiations.[19-22]

Nanoarchitectonics represent an emerging paradigm based on chemical and physical material transformation via dynamic molecular assembly.[23] The advancement of molecular nanoarchitectonics in material science results in the creation of stimuli-responsive dynamic materials, opening pathways to a broad spectrum of applications. This concept can be extended for the customization of the operating temperature of smart windows for different climate conditions. One of the major challenges in the smart window design is the synthesis of copolymers with required molecular weight for controlled particle size formation. A possible solution to some of these problems is the use of thermoresponsive amphiphilic small molecules as the phase change material.[24-29] In this context, amphiphilic π-systems are emerging as an alternative to polymers for the construction of thermoresponsive smart windows.[30,31]

When compared to polyacrylamides, the use of LCST-active small molecular π-systems that are capable of forming supramolecular assemblies have the advantage of defined molecular weight, tuneable optical properties and morphological features by synthetic modifications.[32-36] Nevertheless, such approaches have not been widely exploited for designing smart windows with customizable cloud temperature. Another challenge with smart window design is the autonomous control of the transparency in response to the outdoor light and temperature.[37-40] In order to achieve these objectives, we applied the basic principles of light-induced

[a] Chemical Sciences and Technology Division, CSIR-National Institute for Interdisciplinary Sciences and Technology (CSIR-NIIST), Thiruvananthapuram 695019, India
[b] Academy of Scientific and Innovative Research (AcSIR), Ghaziabad-201002, India
[c] SRM Institute of Science and Technology, Kattankulathur, Chennai 603203, India
E-mail: ajayagha@srmist.edu.in

View Article Online
DOI: 10.1039/D6QM00340K

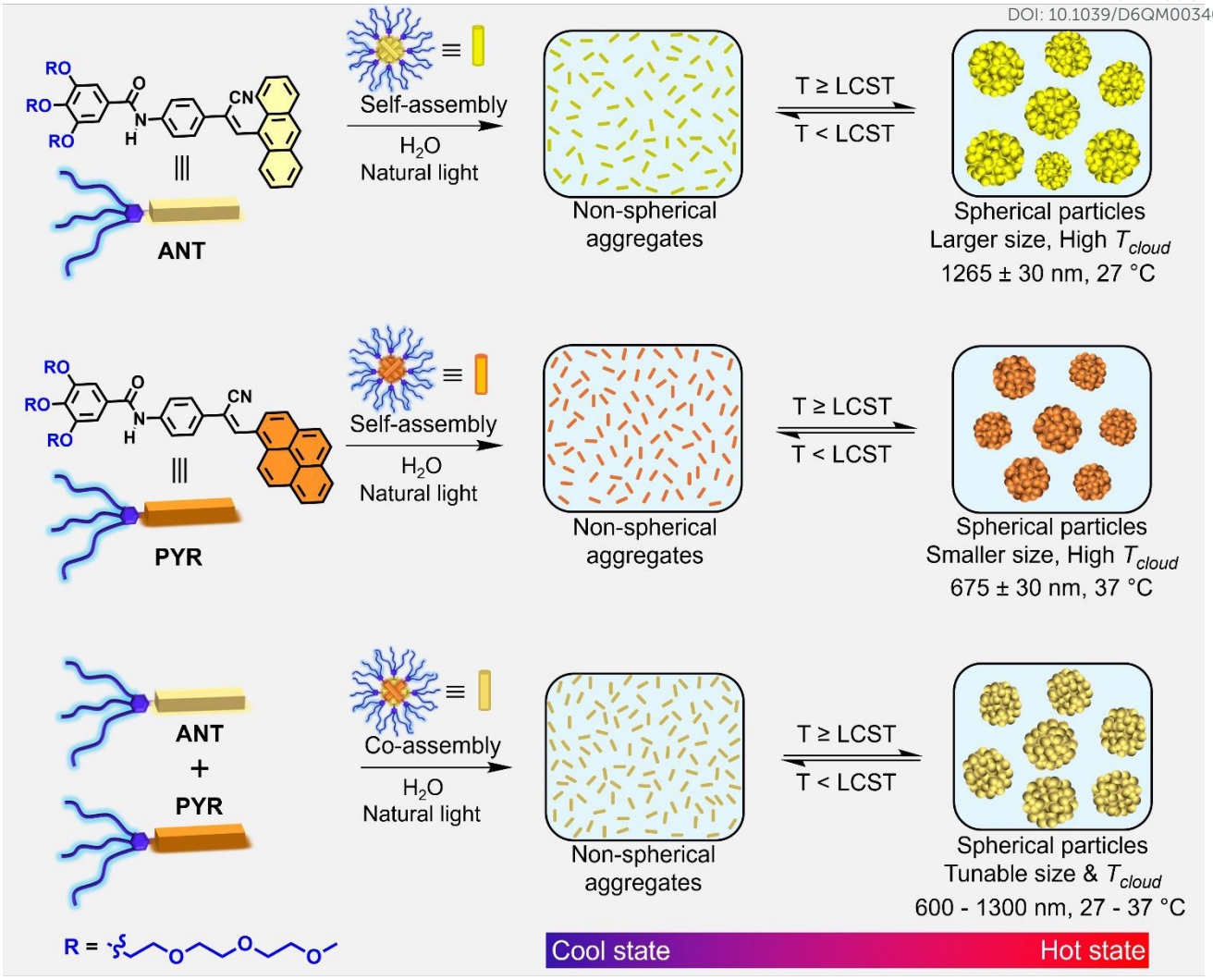

Scheme 1. Schematic illustration of a co-assembly approach for particle size control using two structurally different LCST active amphiphilic π-systems, **ANT** and **PYR**, enabling autonomous transparency modulation. The non-spherical nanoaggregates allow passage of light to appear transparent, whereas the spherical microparticles scatter light to appear opaque.

photoisomerization combined with supramolecular co-assembly of amphiphilic π-systems, leading to significant control on the phase change particle size, thereby regulating the light scattering and the associated transparency modulation.[41-46] Though supramolecular chemistry of small molecular π-systems has been at the center stage of advanced materials research for several decades, they are least exploited for the construction of autonomous thermoresponsive smart windows with customizable cloud temperatures.[47-50]

Herein, we present two small molecular amphiphilic π-systems, **ANT** and **PYR**, exhibiting LCST phenomenon with distinct optical properties and self-assembly behavior as shown in **Scheme 1**. These monomers and their combinations undergo controlled self-assembly/co-assembly in water below their LCST, resulting in transparent solutions consisting of nonspherical nanoaggregates (10-20 nm) as confirmed by the non-sigmoidal DLS correlogram. However, when heated above the LCST, supramolecular agglomeration of the initially formed nanoaggregates to spherical particles of larger size (0.6 -1.3 μm) occurs as established by the sigmoidal correlogram of the DLS spectra, and as a consequence, the solution became opaque. Exposure of the aqueous solutions of the molecules under UV light lowered the T_{cloud} from 27 - 25 °C, in the case of **ANT** and from 37-34 °C in the case of **PYR**. The beauty of the present system is the possible fine-tuning of the particle size during the LCST phase change as per the requirement, by co-assembling with different ratios of **ANT** and **PYR**, allowing the systematic modulation of T_{cloud} between 27-37 °C, a temperature range which is most appropriate for tropical climate. A 10 × 10 cm^2 prototype window can achieve excellent solar light transmittance modulation (79% ΔT_{Solar}, 82% ΔT_{lum}, and 76% ΔT_{IR}) with excellent stability for multiple heating and cooling cycles compared with reported systems in the literatures.[51-53]

View Article Online
DOI: 10.1039/D6QM00340K

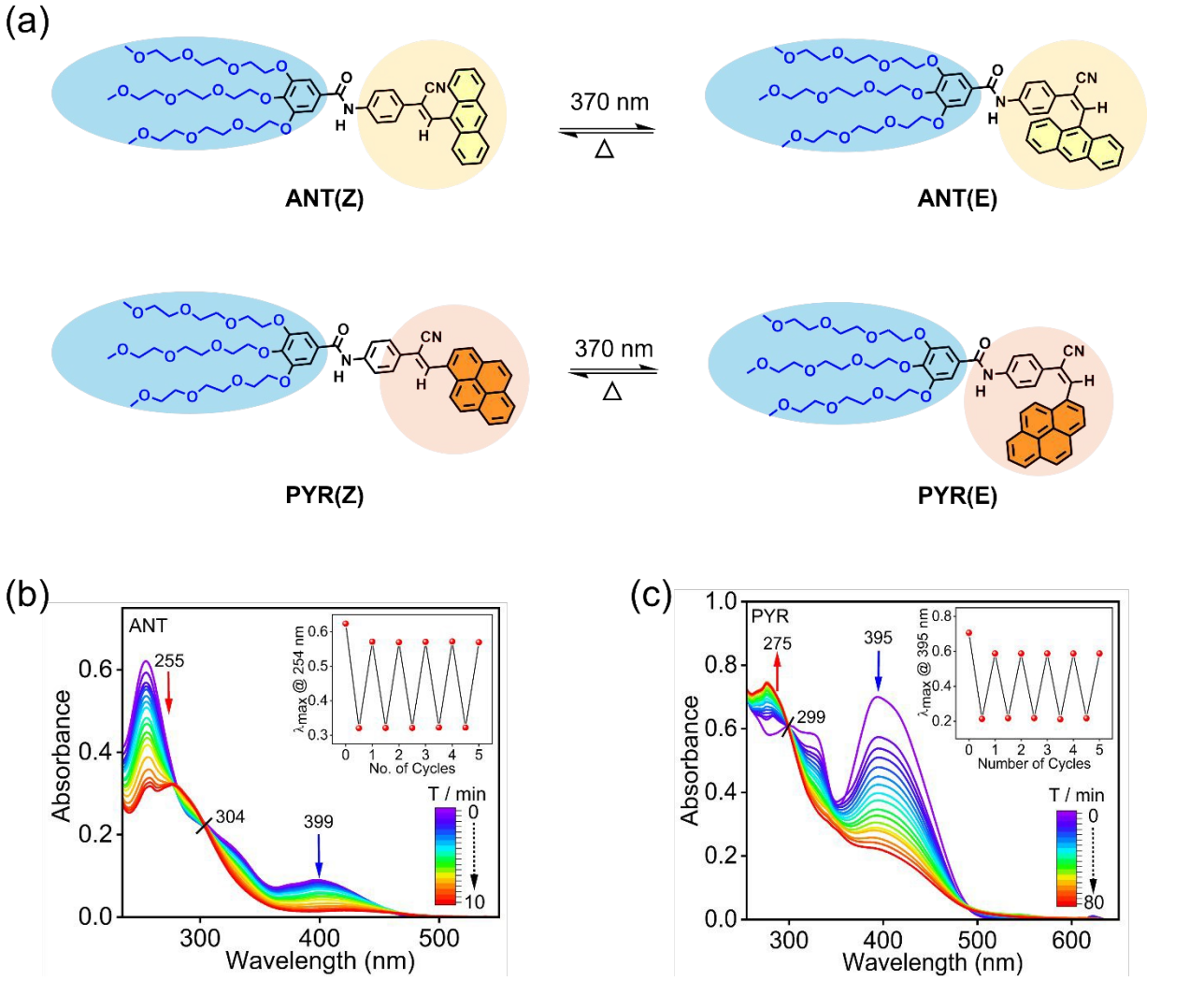

Figure 1. (a) Structures of **ANT(Z)** and **PYR(Z)** and their photoisomerization upon irradiation with 370 nm light. (b), (c) The corresponding changes in the UV-Vis absorption spectra of **ANT(Z)** and **PYR(Z)** in water (c = 5 × 10^{-5} M) respectively. Insets show the respective reversible *Z*/*E*-isomerization under photoirradiation and thermal conditions at the photostationary state.

Results and discussion

We have synthesized two amphiphilic supramolecular π-systems **ANT**, and **PYR** attached with triethylene glycol monomethyl ether chains onto the aromatic core to impart hydrophilicity, aiming at LCST-induced thermoresponsive behavior in water. These molecules were synthesized through the Knoevenagel condensation reaction as per reported procedures (**Scheme S1**)[31] and characterized by spectral analyses (**Figures S31-S38**). Since cyanostilbenes are known to undergo multiple photoreactions such as *Z*/*E*-isomerization, [2+2]-cycloaddition, and Mallory photocyclization, the molecules **ANT**, and **PYR** are carefully chosen in such a way that they undergo exclusively *Z*/*E*-photoisomerization owing to the steric bulkiness of the anthracene and the pyrene moieties (**Figure 1a**).[54-56] The formation of cyclized products was ruled out by the observed reversible change in the time-dependent UV-Vis absorption spectra at elevated temperature (**Figure 1b**, **1c**). The UV-Vis absorption spectra of **ANT**, and **PYR** were recorded in water (c = 5 × 10^{-5} M), which exhibited absorption maxima at 254 and 399 nm for **ANT** and 299 and 395 nm for **PYR**, respectively. UV-Vis, NMR, and FT-IR spectral analyses revealed the formation of molecular assemblies in aqueous medium through intermolecular hydrogen bonding and π–π stacking (**Figure S1-S4**). Upon photoirradiation at 370 nm, both molecules exhibited a gradual decrease in their absorption maxima through an isosbestic point at 304 nm for **ANT** and 299 nm for **PYR**. A photostationary state is achieved within 10 min of irradiation in the case of **ANT**, whereas **PYR** took 80 min to reach the photostationary state, indicating relatively fast isomerization of former when compared to the latter. At the photostationary state, *Z*-isomer of **ANT** is converted to 82% of the *E*-isomer as calculated from the UV-Vis absorption spectral change.

View Article Online
DOI: 10.1039/D6QM00340K

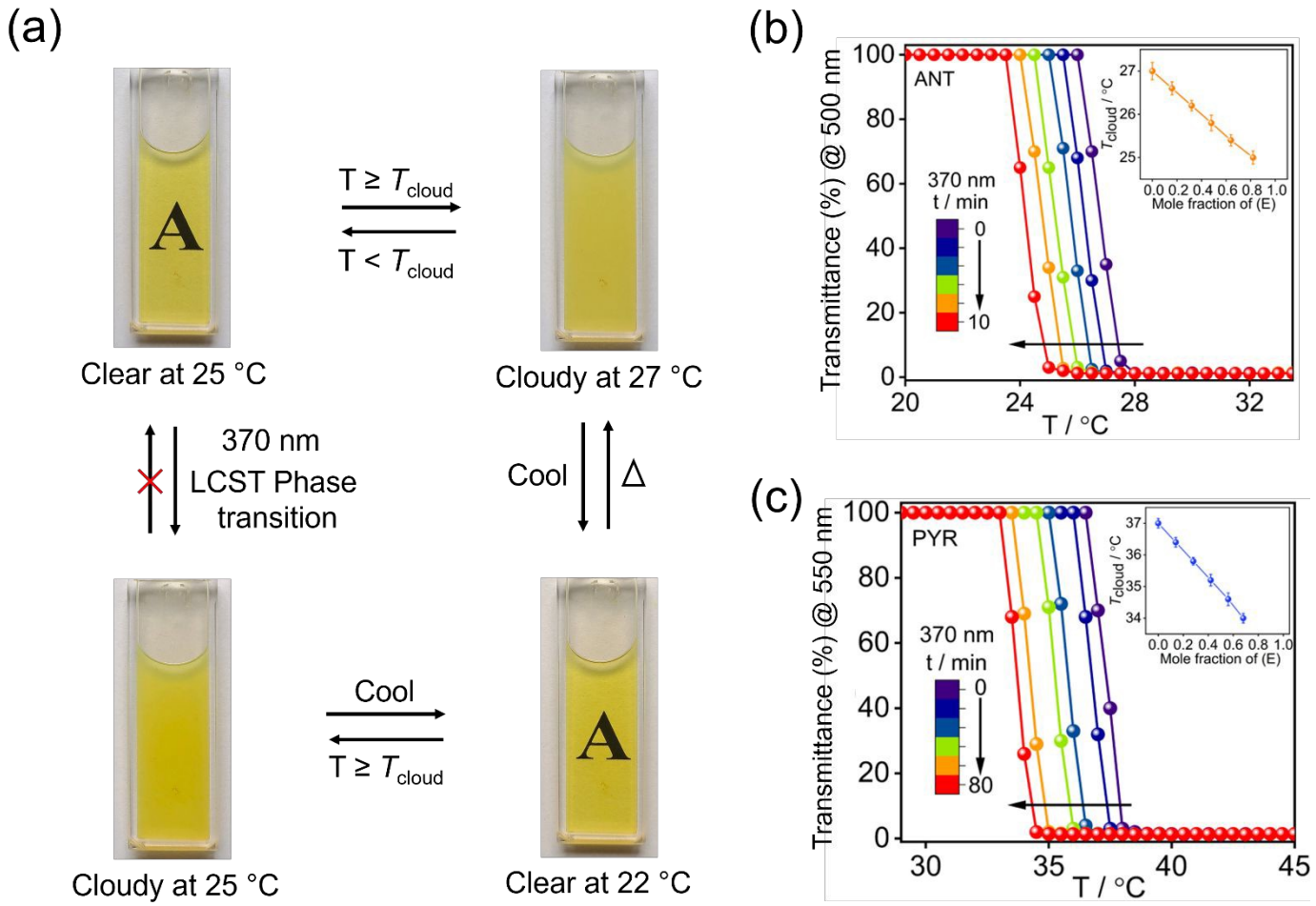

Figure 2. (a) Photographs corresponding to LCST phase transition of **ANT** under photochemical and thermal conditions (The letter '**A**' is visible wherever the solution is transparent). (b), (c) Changes in the light transmittance of **ANT** and **PYR** at different temperatures with continuous irradiation at 370 nm. Insets show the corresponding changes in T_{cloud} with an increase in the mole fraction of *E*-isomer.

Interestingly, in both cases, the thermal back isomerization is found to be sluggish even after keeping the solution under dark for several days, and the solution needed to be heated above 80 °C to observe the reverse isomerization (**Figure S5-S8** and **Table S1-S2**). The isomer ratios for **ANT** were 14:86 (*Z*:*E*) at the photostationary state (PSS) when irradiated at 370 nm (370_{PSS}) and 90:10 (*Z*:*E*) when heated above 80 °C. For **PYR**, the isomer ratios were 30:70 (*Z*:*E*) at the PSS (370 nm) and 84:16 (*Z*:*E*) when heated (above 80 °C). The reversible isomerization plots shown in the insets of **Figure 1b** and **1c** indicate that after the first round of irradiation, a complete thermal recovery of the *Z*-isomers could not be achieved even after prolonged heating, as seen in the UV-Vis spectral change (**Figure S5** and **S6**). Both **ANT** and **PYR** exhibited reversible $Z \rightarrow E$ photoisomerization over multiple cycles, without the sign of photodegradation, demonstrating high fatigue resistance. **ANT** and **PYR** undergo *Z*/*E*-photoisomerization when illuminated by solar light, albeit less efficiently than under 370 nm light (**Figure S9**).

Variable-temperature UV-Vis absorption and ^{1}H NMR spectroscopy revealed the temperature-induced LCST phase transition in water (**Figures S10-S16**). The photographs of the reversible phase change of **ANT** solution are shown in **Figure 2a**. The transparent solution of **ANT** in water (1 mM) turned opaque when heated to 27 °C or when irradiated at 370 nm, which turned cloudy again upon heating above LCST. The temperature-induced phase change and the optical color variation are reversible for heating and cooling processes.

When irradiated to reach photostationary states, the respective solutions turned opaque while maintaining the initial solution temperature, indicating a photoinduced lowering of T_{cloud}. The effect of photoirradiation on LCST phenomenon and the corresponding change in the optical transparency with time of irradiation is shown in **Figures 2b** and **2c**. The insets in **Figure 2b** and **2c** illustrate the corresponding change in T_{cloud} with an increase in the mole fraction of *E*-isomer. In the case of **ANT**, the phase change occurred around 27 °C, whereas **PYR** exhibited a phase change at 37 °C, indicating a difference of 10 °C between the two (**Figure S14** and **S15**). However, in the case of a 1:1 mixture of **ANT** and **PYR**, T_{cloud} appeared around 32 °C (**Figure 3c** and **Figure S16**). The opaque phase is maintained

View Article Online
DOI: 10.1039/D6QM00340K

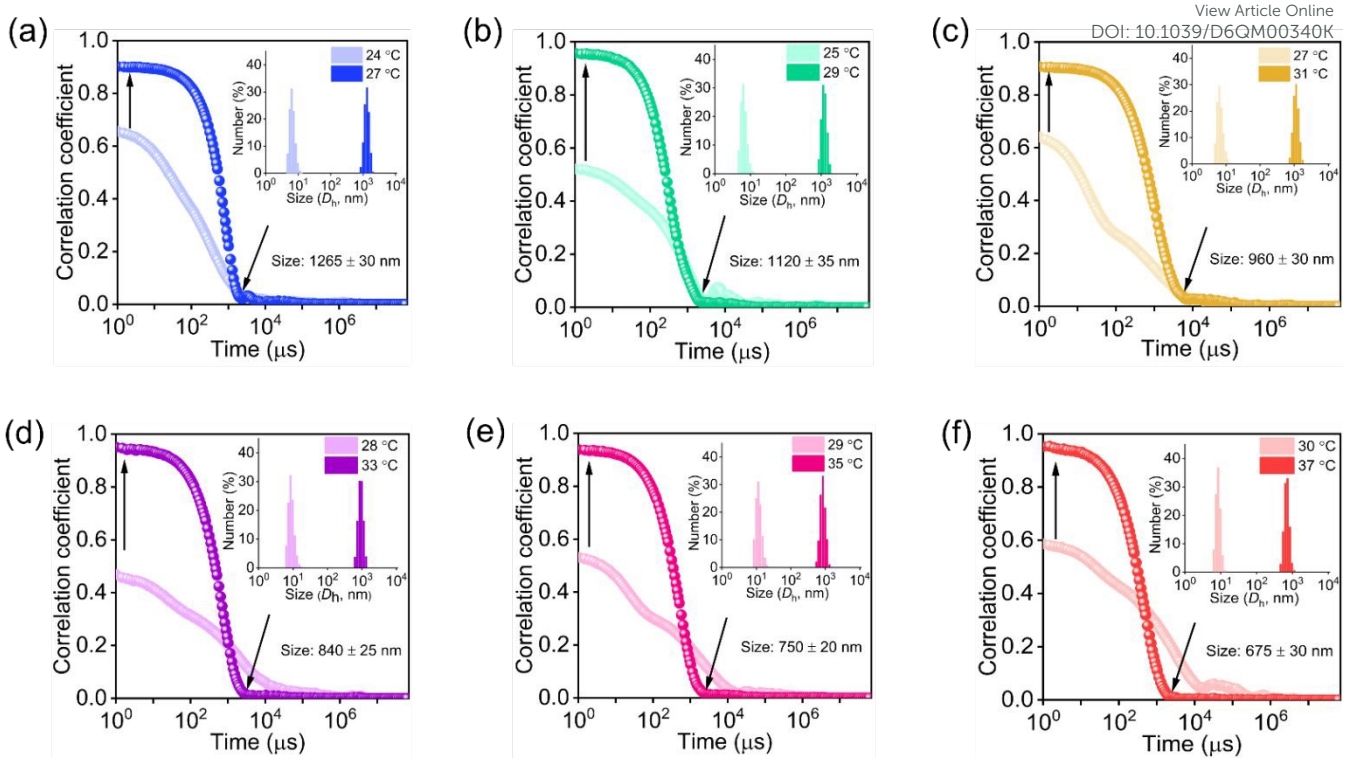

Figure 3. DLS correlation decay profile with time for the co-assembled states: (a) 1:0, (b) 0.8:0.2, (c) 0.6:0.4, (d) 0.4:0.6, (e) 0.2:0.8, (f) 0:1, obtained from ratiometric mixing of **ANT** and **PYR**, respectively below and above cloud point temperatures in water. Insets show DLS plots of the number of particles (%) versus size (D_h, nm) below and above T_{cloud}. The gradual decrease in particle size at their LCST is also shown in the respective figures (inset).

even after keeping the sample for several days in dark, indicating that the back isomerization to *Z*-isomer does not occur and the solution attained equilibrium between the two isomers at the photostationary state. However, when the sample is cooled below its T_{cloud}, it becomes transparent, and further heating above T_{cloud} forces the solution to become cloudy again. To acquire information regarding LCST phase change happening to the molecules, dynamic light scattering (DLS) studies were performed below and above transition temperatures (**Figure 3**) The corresponding particle size distributions are shown in the insets of **Figure 3**. In all cases, DLS data revealed the presence of smaller non-spherical aggregates below the LCST and larger spherical particles above the LCST. DLS data of **ANT** in water (c = 1 mM) before irradiation initially exhibited a particle size of 10-20 nm at 24 °C and 1265 –1300 nm at 27 °C (**Figure 3a**) whereas **PYR** exhibited a particle size of 10-20 nm at 30 °C (below T_{cloud}) and 675 – 700 nm at 37 °C (above T_{cloud}) (**Figure 3f**). In all cases, above LCST, the plots of the correlation coefficients vs time exhibited a sigmoidal curve, which were fitted with a mono-exponential decay function, suggesting the formation of larger spherical particles, resulting in strong light-scattering abilities. These observations are in agreement with light scattering principle, where correlogram corresponding to DLS spectrum is the signature of a non-spherical to spherical particle formation during the LCST phase change. LCST parameters, such as concentration-dependent transmittance, T_{cloud}, particle size variations, and thermal hysteresis of **ANT**, **PYR** and **ANT**/**PYR** (1:1) are shown in **Figure S14-S16**, respectively. In both cases, after photoirradiation, DLS data exhibited a slight increase in particle size above their respective T_{cloud} values, which is in agreement with observed decrease in their respective T_{cloud} values (**Figure S17**).

Customization of the operating temperature and transparency to meet a specific climate condition are the difficult challenges in the design of smart windows. Though supramolecular co-assembly of LCST active molecules has been shown to influence on their T_{cloud}, this approach has not been tested for the construction of smart windows.[57] We have successfully implemented this strategy to modulate the T_{cloud} of **ANT** and **PYR** in response to the ambient weather conditions for designing thermoresponsive smart windows. For this purpose, co-assemblies of **ANT** and **PYR** were prepared in different mole ratios in water at around 20 °C. It is found that the T_{cloud} values of the co-assembly systematically vary between the T_{cloud} values of **ANT** and **PYR** upon changing their mole ratios (**Figure 4a**). T_{cloud} is found to decrease with an increase in **ANT** content in the co-assembly, as seen when the transition temperature is plotted against the variation in the mole ratio (**Figure 4b**). Interestingly, the DLS analysis of the co-assembly at different **ANT**/**PYR** compositions revealed the formation of spherical particles above their T_{cloud} values with a significant increase in the hydrodynamic radius as the mole fraction of **ANT** is increased (**Figure 3** and **Figure 4c**). A dynamic change in the particle size between 675 and 1300 nm at different compositions could be observed, where the particles collapse at lower temperature and reform at a higher temperature (**Figure**

View Article Online
DOI: 10.1039/D6QM00340K

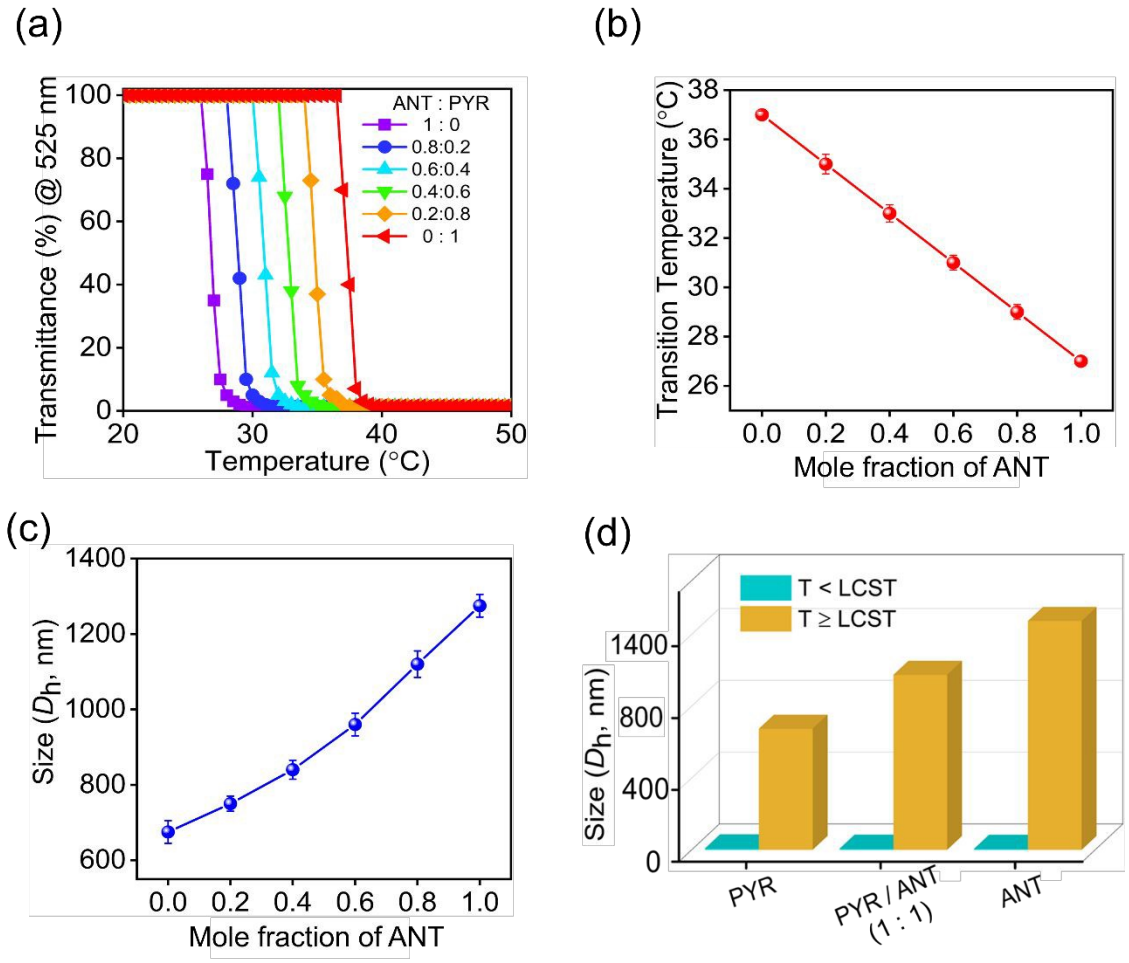

Figure 4. Plots of LCST parameters at various compositions of **ANT** and **PYR**. (a) % Transmittance vs temperature, b) T_{cloud} vs **ANT**/**PYR** ratio, c) hydrodynamic diameter vs **ANT**/**PYR** ratio and d) variation of hydrodynamic diameter at different **ANT**/**PYR** ratios, below and above LCST.

4d). The thermal hysteresis of co-assembled **ANT**/**PYR** at different mixing ratios were found to be almost identical (**Figure S18**). LCST phenomenon and the phase change arise from the interplay between hydrophilic–hydrophobic balance and intrinsic dipole moments of *Z*/*E*-isomers.[58,59] According to DFT analysis, *Z*-isomer displays a markedly increased dipole moment relative to *E*-isomer in both **ANT** and **PYR** derivatives (**Figure S19-S22** and **Table S3**). Consequently, T_{cloud} of *Z*-isomer is higher than that of *E*-isomer. After evaluating LCST phenomenon of **ANT**, **PYR** and their combination (1:1 molar ratio), we have fabricated 10 × 10 cm^2 smart window prototypes using 1 mM aqueous solutions (**Figure 5**). The window fabricated with **ANT** exhibited transparent-to-opaque switching at 28 °C with a light greenish yellow color tone and remained opaque with a further increase in temperature (**Figure 5a** and **Movie S1**). However, the window fabricated with **PYR** remained transparent till 32 °C and turned opaque at 38 °C, showing a 10°C difference in cloud point temperature (**Figure 5c and Movie S2**). In this case the color tone of window appeared as golden yellow. On the other hand, the window fabricated with a 1:1 mole ratio of **ANT** and **PYR** turned opaque at 32 °C with a color tone of light yellow (**Figure 5b** and **Movie S3**). The CIE chromaticity diagram, along with the window's color coordinates below and above LCST, is shown in **Figure S23**. The stability of the windows was tested initially for a 24 h time period between their cloud temperatures by plotting the transmittance spectra vs time (**Figure S24**) and then the process was repeated for multiple cycles of operations. The corresponding plots are shown on the side of the respective window in **Figure 5**. These plots reveal high thermal stability of the windows for a wide range of tropical temperatures. The variable-temperature transmittance spectra of **ANT** displayed notably rapid switching times, with a fast response of 10 ± 1 sec. for transition from transparent to opaque state during heating, and the cooling cycles recorded within 21 ± 2 sec. (**Figure S25a**). In comparison, **PYR** exhibited slightly slower switching characteristics, with heating and cooling cycles recorded within 13 ± 2 sec. and 30 ± 4 sec., respectively (**Figure S25b**). The optical transmittance spectra of the **ANT** window, below and above the cloud temperature in comparison to the solar transmittance spectrum is shown in **Figure 6a**. The optical transparency of the window showed 84%

View Article Online
DOI: 10.1039/D6QM00340K

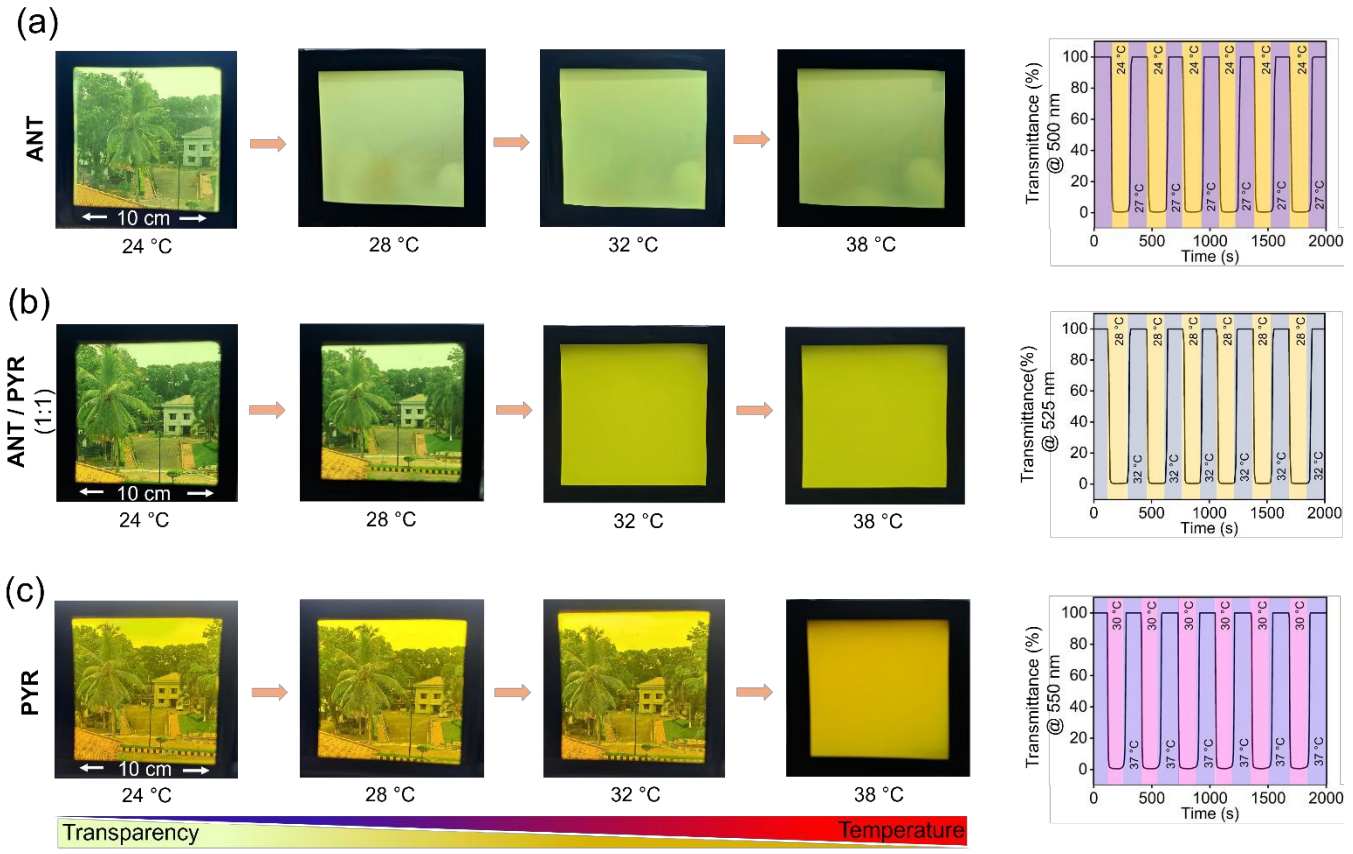

Figure 5. Solar light-induced transparency modulation of 10 × 10 cm² smart window prototypes between 24-38 °C and their respective transparency switching operations below and above T_{cloud}. (a) **ANT**, (b) **ANT/PYR** (1:1), and (c) **PYR**. The outdoor solar light intensity was 1 × 10³ W/m².

transmittance in the visible region (400-780 nm) at 20 °C and 1.7% transmittance at 27 °C. Upon increasing temperature to 27 °C, the window turned opaque with a greenish-yellow color tone, and the transmittance of solar light approached to zero in the UV-Vis-NIR (400-2500 nm) region (**Figure 6a**). Notably, the **ANT** windows exhibited higher solar transmittance (T_{Solar}), and luminous transmittance (T_{lum}) at low temperatures in comparison with **PYR** windows, whereas T_{IR} transmittance remained almost same in both cases (**Figure 6b** and **Figure S26**). The stability and consistency of the window in transmitting solar light is further established by plotting the T_{Solar} and transmittance modulation (% ΔT) for multiple switching cycles of 1000 times below and above T_{cloud} (**Figure 6c** and **6d**). More importantly, even after 10,000 cycles of operations, the transmittance remained almost constant at temperature variations of below and above the cloud point temperatures (**Figure 6e** and **Figure S27**). Variable-temperature DLS data revealed that hydrodynamic diameters of **ANT**, **PYR**, and **ANT**:**PYR** (1:1) particles remain unchanged even after multiple heating and cooling cycles, indicating excellent long-term stability in water (**Figure S28**). The combined transmittance performance in both transparent and opaque states under indoor temperature regulation makes **ANT**, **PYR**, and their co-assembled state promising candidates for smart window applications, offering advantages over conventional thermochromic inorganic, organic, and polymer materials (**Figure 6f**). Finally, from the application viewpoint, we have fabricated a library of smart window prototypes by a mix-and-match approach, which is usually applied for screening a large number of molecules and materials for specific applications. Four different types of smart window panels using **ANT**, **ANT**/**PYR** (1:1), **PYR**, and their combinations, namely **A**, **B**, **C**, and **D** respectively, were fabricated and their performance were evaluated for a temperature range of 24-38 °C (**Figure S29**). All modules in window A are fabricated with **ANT**, modules in B with **ANT**/**PYR** (1:1) and modules in C with **PYR**, whereas all modules in window D are made up of a combination of **ANT**, **ANT**/**PYR** (1:1), and **PYR**. It can be seen that all modules in window A are transparent at 24 °C and turn opaque at 28 °C and above. When the window panels were fabricated with modules having a 1:1 combination of **ANT**/**PYR** as in B, they exhibited a thermal response at 32 °C and above. All modules in window 'C' are transparent up to 35 °C and turn opaque at 38 °C. It is possible to prepare a number of window modules that respond systematically to temperatures in between 24-38 °C, using different supramolecular combinations of **ANT**/**PYR**, thus

View Article Online
DOI: 10.1039/D6QM00340K

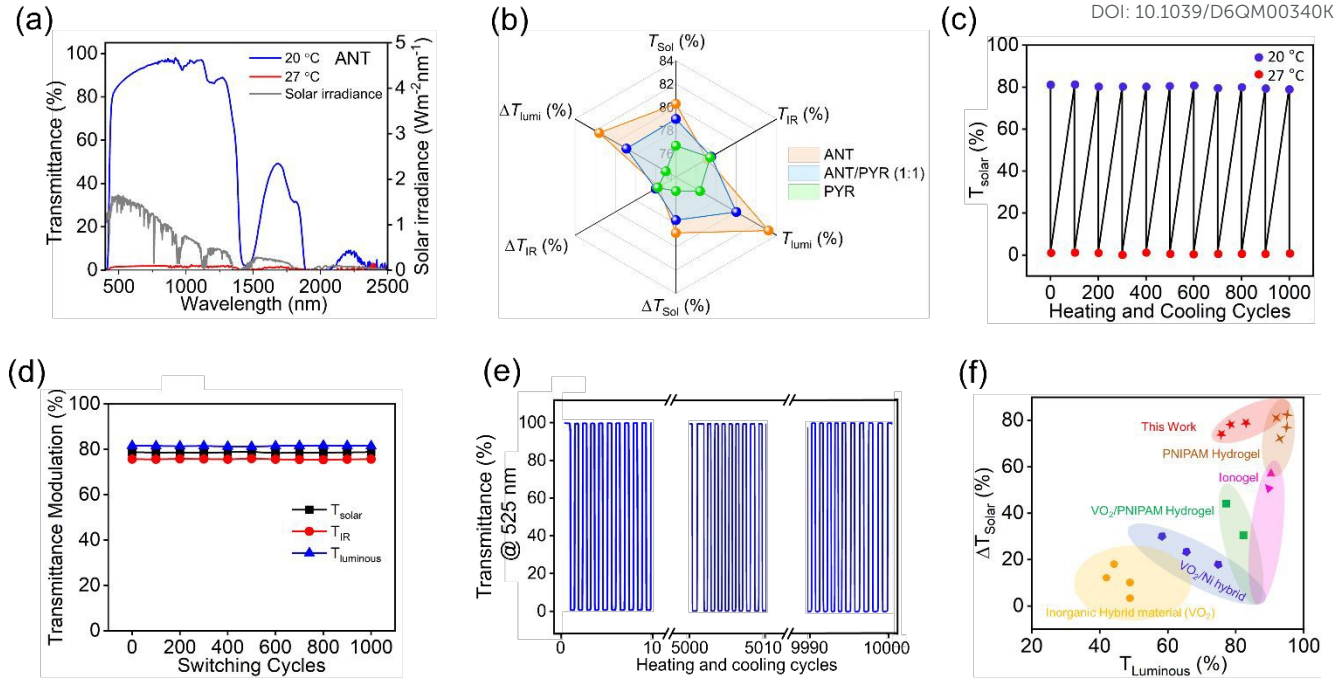

Figure 6. Solar radiation control performance of a 10 × 10 cm^2 smart window prototype fabricated with **ANT**. (a) Light transmittance spectra at above and below the LCST in comparison with the solar radiation spectrum. (b) Solar light scattering pattern of **ANT** in comparison with **PYR** and **ANT/PYR** (1:1). (c), (d) Reversible solar transmittance and stable transmittance modulation for 1000 switching cycles. e) Shelf-life of the window **ANT/PYR** (1:1) after 10,000 cycles below and above T_{cloud}. (f) Thermochromic performance of the smart window prototypes in this study compared with reported systems in the literatures.

providing opportunities to construct a combinatorial library of smart windows that can autonomously change the transparency and color tones. In addition, window panels having different modules of **ANT**, **PYR** and **ANT/PYR** combinations can be constructed as shown in panel '**D**'. The thermal response of panel '**D**' at different temperatures is shown. At 24 °C, all modules are transparent, allowing maximum transparency. When the temperature is raised to 28 °C, **ANT** module becomes opaque, thereby reducing light transmittance by 1/3. Upon further increasing the temperature to 32 °C, **PYR** module will remain transparent, and the other two become opaque, thus reducing the light transmittance to 2/3. At 38 °C, all modules become opaque with maximum blocking of light. Thus, windows constructed using panel **D** can autonomously control the transparency and color tones with the dynamic variations in atmospheric temperature, which in turn can regulate light and temperature in an indoor space. Further, window panels **A**, **B**, **C**, and **D** provide multiple options to construct a variety of combinatorial modules by changing the percentage of **ANT** and **PYR** in supramolecular co-assembly mixture. In this way, '16' number of combinatorial window modules in four types of arrangements with **A**, **B**, **C**, and **D** can be constructed using a mix-and-match approach.

Further mix-and-match can create another '64' combinations as shown in **Figure S30**. In principle, with the imagination and creativity of a user, any number of window combinations become possible for the construction of large area glass window facades. These window facades are aesthetically appealing and can autonomously modulate their cloud temperature and the light intensity in a closed space in response to external temperature. The outcome of such windows when integrated into building architecture is significant energy saving by reducing the energy required for air conditioning, in addition to their aesthetic appeal. The technology development studies for potential commercial application of the described smart windows are in progress.

Conclusions

The amphiphilic π-systems **ANT** and **PYR** reported here exhibit LCST phenomenon with phase transition cloud temperature of 27 and 37 °C respectively. The cloud point temperature of these molecules could be controlled by photoisomerization and supramolecular co-assembly. Since there is a 10 °C difference in the T_{cloud} of **ANT** and **PYR**, supramolecular co-assembly of these molecules at different mole ratios allowed regulation of the solar radiation transmittance over a range of 27-37 °C. The supramolecular phase change and the associated particle size variation above T_{cloud} is crucial in controlling the light scattering, thereby autonomously controlling the light transmittance. Prototype (10 × 10 cm^2) windows fabricated with **ANT**, **PYR**, and **ANT/PYR** (1:1 ratio) exhibited significant changes in solar (81% - 1.7%), luminous (84% - 1.6%), and thermal IR transmittance (78% - 1.8%) during the transparent-to-opaque phase transition at their respective cloud temperatures. Tuning of the cloud temperature by the supramolecular co-assembly approach described here allows the construction of a large number of custom-made smart windows suitable for tropical climates. In

conclusion, the described LCST-active supramolecular π-systems can be effectively used as excellent thermoresponsive functional materials for the construction of smart windows that are self-adaptive to the atmospheric temperature and solar radiation.

Author contributions

D.P. has undertaken the synthesis and characterization of the target molecules and performed the experimental work. D.P and A.G. have designed the experiments, discussed the results, analyzed the data, and co-wrote the manuscript. A.G. was responsible for the overall project concept, direction, coordination and project funding.

Conflicts of interest

There are no conflicts of interest to declare.

Data availability

The authors declare that data supporting the findings of this study are available within the paper and its supplementary information (SI). The data is available from the authors on request.

Acknowledgements

D.P is thankful to CSIR for a research fellowship and A.A is grateful to CSIR for a Bhatnagar Fellowship grant (CSIRHRD/BFS 2024/03/03).

Notes and references

1 J. D. Kocher, A Mahfouz, J. G. McDaniel, A. K. Menon, Thermodynamic properties of lower critical solution temperature (LCST) mixtures for application in energy–water systems, *Phys. Chem. Chem. Phys.*, 2025, **27**, 15024.
2 A. Agarwal, B. G. Bobay, M. L. Becker, Observation of Dynamic Aggregation Behavior in Thermoresponsive Micro-and Nanoparticles via Diffusion-Ordered NMR Spectroscopy, *J. Am. Chem. Soc.*, 2025, **147**, 9386–9395.
3 S. S. Chittari, A. C. Obermeyer, A. S. Knight, Investigating Fundamental Principles of Nonequilibrium Assembly Using Temperature-Sensitive Copolymers, *J. Am. Chem. Soc*., 2023, **145**, 6554–6561.
4 V. R. de la Rosa, P. Woisel, R. Hoogenboom, Supramolecular control over thermoresponsive polymers, *Mater. Today*, 2016, **19**, 44–55.
5 K. Ryu, G. Li, K. Zhang, J. Guan, Y. Long, Z. Dong, Thermoresponsive Hydrogels for the Construction of Smart Windows, Sensors, and Actuators, *Acc. Mater. Res.*, 2025, **6**, 379–392.
6 D. Patra, R. D. Mukhopadhyay, A. Ajayaghosh, Lower Critical Solution Temperature Active Supramolecular π-Systems for Smart Applications, *Angew. Chem. Int. Ed*., 2025, **137**, e202517868.
7 J. Korpanty, L. R. Parent, N. Hampu, S. Weigand, N. C. Gianneschi, Thermoresponsive polymer assemblies via variable temperature liquid-phase transmission electron microscopy and small angle X-ray scattering, *Nat. Commun.*, 2021, **12**, 6568.
8 S. Wu, Q. Zhang, Y. Deng, X. Li, Z. Luo, B. Zheng, S. Dong, Assembly Pattern of Supramolecular Hydrogel Induced by Lower Critical Solution Temperature Behavior of Low-Molecular-Weight Gelator, *J. Am. Chem. Soc*., 2020, **142**, 448–455.
9 W. Chen, Z. Lin, S. Hu, An All-Weather Sol–Gel Thermochromic Energy-Saving Smart Window, *ACS Appl. Mater. Interfaces*, 2024, **16**, 70863−70873.
10 G. Chen, K. Wang, J. Yang, J. Huang, Z. Chen, J. Zheng, J. Wang, H. Yang, S. Li, Y. Miao, W. Wang, N. Zhu, X. Jiang, Y. Chen, J. Fu, Printable Thermochromic Hydrogel-Based Smart Window for All-Weather Building Temperature Regulation in Diverse Climates, *Adv. Mater.*, 2023, **35**, 2211716.
11 X. H. Li, C. Liu, S. P. Feng, N. X. Fang, Broadband Light Management with Thermochromic Hydrogel Microparticles for Smart Windows, *Joule*, 2019, **3**, 290–302.
12 Z. Du, S. Wang, C. Gu, G. Yang, Recent advances in photo- or electro-chromic smart windows and their thermal regulation, *Responsive Mater*., 2025, **3**, e20250007.
13 M. J. Moran, M. Magrini, D. M. Walba, I. Aprahamian, Driving a Liquid Crystal Phase Transition Using a Photochromic Hydrazone, *J. Am. Chem. Soc*., 2018, **140**, 13623–13627.
14 H. Khandelwal, A. P. H. J. Schenning, M. G. Debije, Infrared Regulating Smart Window Based on Organic Materials, *Adv. Energy Mater.*, 2017, **7**, 1602209.
15 Z. Zhang, L. Zhang, Y. Zhou, Y. Cui, Z. Chen, Y. Liu, J. Li, Y. Long, Y. Gao, Thermochromic Energy Efficient Windows: Fundamentals, Recent Advances, and Perspectives, *Chem. Rev.*, 2023, **123**, 7025–7080.
16 A. Nirmala, I. Mukkatt, S. Shankar, A. Ajayaghosh, Thermochromic Color Switching to Temperature Controlled Volatile Memory and Counter Operations with Metal–Organic Complexes and Hybrid Gels, *Angew. Chem. Int. Ed*., 2021, **60**, 455-465.
17 L. Gonzalez, C. Liu, B. Dietrich, H. Su, S. Sproules, H. Cui, D. Honecker, D. J. Adams, E. R. Draper, Transparent-to-dark photo- and electrochromic gels, *Commun. Chem.,* 2018, **1**, 77.
18 S. Wang, Z. Xu, T. Wang, T. Xiao, X.-Y. Hu, Y.-Z. Shen, L. Wang, Warm/cool-tone switchable thermochromic material for smart windows by orthogonally integrating properties of pillar[6]arene and ferrocene, *Nat. Commun*., 2018, **9**, 1737.
19 J. Li, P. Gu, H. Pan, Z. Qiao, J. Wang, Y. Cao, W. Wang, Y. Yang, A Facile yet Versatile Strategy to Construct Liquid Hybrid Energy-Saving Windows for Strong Solar Modulation, *Adv. Sci*., 2023, **10**, 2206044.
20 K. Zhang, M. Zhang, X. Feng, M. A. Hempenius, G. J. Vancso, Switching Light Transmittance by Responsive Organometallic Poly(ionic liquid)s: Control by Cross Talk of Thermal and Redox Stimuli, *Adv. Funct. Mater.,* 2017, **27**, 1702784.
21 G. Xu, H. Xia, P. Chen, W. She, H. Zhang, J. Ma, Q. Ruan, Thermochromic Hydrogels with Dynamic Solar Modulation and Regulatable Critical Response Temperature for Energy-Saving Smart Windows, *Adv. Funct. Mater.,* 2021, **32**, 2109597.
22 Q. Zhang, Y. Jiang, L. Chen, W. Chen, J. Li, Y. Cai, C. Ma, W. Xu, Y. Lu, X. Jia, Z. Bao, Ultra-Compliant and Tough Thermochromic Polymer for Self-Regulated Smart Windows, *Adv. Funct. Mater*., 2021, **31**, 2100686.
23 K. Ariga, Nanoarchitectonics: the method for everything in materials science, *Bull. Chem. Soc. Jpn*., 2024, **97**, uoad001.
24 F. D. Jochum, P. Theato, Temperature- and light-responsive smart polymer materials, *Chem. Soc. Rev.*, 2013, **42**, 7468–7483.
25 X. Chi, G. Yu, L. Shao, J. Chen, F. Huang, A Dual-Thermoresponsive Gemini-Type Supra-amphiphilic

Macromolecular [3]Pseudorotaxane Based on Pillar[10]arene/Paraquat Cooperative Complexation, *J. Am. Chem. Soc.*, 2016, **138**, 3168–3174.
26 T. Yuan, M. Vazquez, A. N. Goldner, Y. Xu, R. Contrucci, M. A. Firestone, M. A. Olson, L. Fang, Versatile Thermochromic Supramolecular Materials Based on Competing Charge Transfer Interactions, *Adv. Funct. Mater*., 2016, **26**, 8604–8612.
27 P. Wei, T. R. Cook, X. Yan, F. Huang, P. J. Stang, A Discrete Amphiphilic Organoplatinum(II) Metallacycle with Tunable Lower Critical Solution Temperature Behavior, *J. Am. Chem. Soc*., 2014, **136**, 15497–15500.
28 Y. Yang, A. J. Mijalis, H. Fu, C. Agosto, K. J. Tan, J. D. Batteas, D. E. Bergbreiter, Reversible Changes in Solution pH Resulting from Changes in Thermoresponsive Polymer Solubility, *J. Am. Chem. Soc.*, 2012, **134**, 7378–7383.
29 K. Belal, F. Stoffelbach, J. Lyskawa, M. Fumagalli, D. Hourdet, A. Marcellan, L. De Smet, V. R. de la Rosa, G. Cooke, R. Hoogenboom, P. Woisel, Recognition-Mediated Hydrogel Swelling Controlled by Interaction with a Negative Thermoresponsive LCST Polymer, *Angew. Chem. Int. Ed*., 2016, **128**, 14180–14184.
30 S. Das, D. Patra, S. Shankar, A. Ajayaghosh, Photocycloaddition as a Tool for Modulation of the Lower Critical Solution Temperature in a Molecular π-System to Control Transmission of Solar Radiation, *Angew. Chem. Int. Ed*., 2022, **61**, e202207641.
31 D. Patra, S. Das, S. Shankar, A. Ajayaghosh, The Nanoarchitectonics of Sustainable Smart Window Design by LCST Modulation of Photoresponsive Molecular π-Systems, *Adv. Funct. Mater.*, 2024, **34**, 2408014.
32 H.-Q. Peng, B. Liu, P. Wei, P. Zhang, H. Zhang, J. Zhang, K. Li, Y. Li, Y. Cheng, J. W. Y. Lam, W. Zhang, C.-S. Lee, B. Z. Tang, Visualizing the Initial Step of Self-Assembly and the Phase Transition by Stereogenic Amphiphiles with Aggregation-Induced Emission, *ACS Nano*, 2019, **13**, 839–846.
33 G. J. Richards, J. Labuta, J. P. Hill, T. Mori, K. Ariga, Designing Lower Critical Solution Temperature Behavior into a Discotic Small Molecule, *J. Phys. Chem. Lett.,* 2010, **1**, 1336–1340.
34 J. Zhou, W. Yuan, Y. Qing, G. Du, Q. Li, A Coordinating Small Organic Molecule with Tunable Lower Critical Solution Temperature for Efficient Management of Solar Radiation, *Macromol. Rapid Commun.,* 2024, **45**, 2400167.
35 Y.H. Chu, M. F. Cheng, Y. H. Chiang, Combinatorial discovery of small-molecule 1,2,3-triazolium ionic liquids exhibiting lower critical solution temperature phase transition, *Sci. Rep.,* 2020, **10**, 18247.
36 M. A. Martínez, D. Aranda, E. Ortí, J. Aragó, L. Sánchez, Thermodynamics of the self-assembly of N-annulated perylene bisimides in water. Disentangling the enthalpic and entropic contributions, *Org. Chem. Front.*, 2023, **10**, 1959–1967.
37 X. Li, X. Bu, J. Huang, Y. Li, L. Wang, H. Miao, G. Shi, A long-term stable thermochromic smart window of PNIPAM-based hydrogels with excellent water retention and visible light modulation, *J. Mater. Chem. A,* 2026, **14**, 10657-10667.
38 F. Jiang, K. Yu, R. Kieffer, D. d. Jong, R. M. Parker, S. Vignolini, M. E. A. Tam, Thermochromic hydrogel with high transmittance modulation and fast response for flexible smart windows, *Commun. Mater.*, 2025, **6**, 239.
39 G. Li, J. Chen, Z. Yan, S. Wang, Y. Ke, W. Luo, H. Ma, J. Guan, Y. Long, Physical crosslinked hydrogel-derived smart windows: anti-freezing and fast thermal responsive performance, *Mater. Horiz*., 2023, **10**, 2004–2012.
40 K. Wang, S. Liu, J. Yu, P. Hong, W. Wang, W. Cai, J. Huang, X. Jiang, Y. Lai, Z. Lin, Hofmeister Effect-Enhanced, Nanoparticle-Shielded, Thermally Stable Hydrogels for Anti-UV, Fast-Response, and All-Day-Modulated Smart Windows, *Adv. Mater*., 2025, **37**, 2418372.
41 T. Ogoshi, K. Kida, T. A. Yamagishi, Photoreversible Switching of the Lower Critical Solution Temperature in a Photoresponsive Host–Guest System of Pillar[6]arene with Triethylene Oxide Substituents and an Azobenzene Derivative, *J. Am. Chem. Soc.*, 2012, **134**, 20146–20150.
42 T. Dünnebacke, K. K. Kartha, J. M. Wiest, R. Q. Albuquerque, G. Fernández, Solvent-controlled *E/Z* isomerization vs. [2 + 2] photocycloaddition mediated by supramolecular polymerization, *Chem. Sci.*, 2020, **11**, 10405–10413.
43 L. B. Zou, X. L. Zhou, H. Zheng, Z. W. Fan, D. W. Pan, Z. Liu, W. Wang, R. Xie, X. J. Ju, L. Y. Chu, Regulatory effects of cyclodextrins on light-responsive phase transition behaviors ofpoly(N-isopropylacrylamide-co-N-(4-phenylazophenyl)-methylacrylamide), *Polymer*, 2024, **313**, 127676.
44 J. Cui, J. E. Kwon, H.-J. Kim, D. R. Whang, S. Y. Park, Smart Fluorescent Nanoparticles in Water Showing Temperature-Dependent Ratiometric Fluorescence Color Change, *ACS Appl. Mater. Interfaces*, 2017, **9**, 2883–2890.
45 C. Li, A. Ke, H. Shen, X. Zhang, Photonic crystal-integrated thermo-responsive smart windows with multicolor and enhanced NIR shielding, *J. Mater. Chem. A*, 2025, **13**, 18833–18841.
46 Y. Ding, Z. Wang, X. Zhang, Thermosensitive micelles formed from a small-molecule amphiphile: switchable LCST and potential application in cloud point separation, *Chem. Commun.*, 2013, **49**, 5580–5582.
47 P. P. N. Syamala, F. Würthner, Modulation of the Self-Assembly of π-Amphiphiles in Water from Enthalpy-to Entropy-Driven by Enwrapping Substituents, *Chem. Eur. J.,* 2020, **26**, 8426–8434.
48 Y. Deng, X. Li, Q. Zhang, Z. Luo, C. Han, S. Dong, LCST phase behavior of benzo-21-crown-7 with different alkyl chains, *Beilstein J. Org. Chem*., 2019, **15**, 437-444.
49 S. Dong, J. Heyda, J. Yuanc, C. A. Schalley, Lower critical solution temperature (LCST) phase behaviour of an ionic liquid and its control by supramolecular host–guest interactions, *Chem. Commun*., 2016, **52**, 7970–7973.
50 P. P. N. Syamala, B. Soberats, D. Görl, S. Gekle, F. Würthner, Thermodynamic insights into the entropically driven self-assembly of amphiphilic dyes in water, *Chem. Sci.*, 2019, **10**, 9358–9366.
51 S. Wu, H. Sun, M. Duan, H. Mao, Y. Wu, H. Zhao, Applications of thermochromic and electrochromic smart windows: Materials to buildings, *Cell Reports Phys. Sci.* 2023, **4**, 101370.
52 D. Wang, G. Chen, J. Fu, Multifunctional thermochromic smart windows for building energy saving, *J. Mater. Chem. A*, 2024, **12**, 12960-12982.
53 K. Lei, Q. Jiang, D. Gong, W. Wang, J. Wu, Q. Chang, G. Wang, X. Pang, Hydrogel Smart Windows: Working Mechanisms, Recent Developments, and Perspectives, *Small*, 2025, **21**, e10382.
54 P. Wei, J.-X. Zhang, Z. Zhao, Y. Chen, X. He, M. Chen, J. Gong, H. H. Y. Sung, I. D. Williams, J. W. Y. Lam, B. Z. Tang, Multiple yet Controllable Photoswitching in a Single AIEgen System, *J. Am. Chem. Soc.*, 2018, **140**, 1966–1975.
55 Y. Shao, W. Li, M. Cametti, Z. Džolić, Z. Ding, Z. Yang, Y. Xie, S. Jiang, Single-Component High-Performance Adhesives Enabled by Synergistic Supramolecular and Covalent Polymerization, *J. Am. Chem. Soc.*, 2025, **147**, 23868–23877.
56 N. F. König, D. Mutruc, S. Hecht, Accelerated Discovery of α-Cyanodiarylethene Photoswitches, *J. Am. Chem. Soc.,* 2021, **143**, 9162–9168.
57 D. Görl, B. Soberats, S. Herbst, V. Stepanenko, F. Würthner, Perylene bisimide hydrogels and lyotropic liquid crystals with temperature-responsive color change, *Chem. Sci.,* 2016, **7**, 6786-6790.

View Article Online
DOI: 10.1039/D6QM00340K

58 R. Colaco, C. Appiah, A. Staubitz, Controlling the LCST-Phase Transition in Azobenzene-Functionalized Poly(N-Isopropylacrlyamide) Hydrogels by Light, *Gels*, 2023, **9**, 75.
59 R. Colaco, N. Wolf, P. Hepke, R. Renken, A. Staubitz, Superswelling, Supershrinking, and a Broadened Phase Transition–Amphiphilic Thermosensitivity in Sulfonate-Functionalized Azobenzene-co-NIPAAm Hydrogels and Polymers, *ACS Appl. Polym. Mater.,* 2025, **7**, 13896–13906.

View Article Online
DOI: 10.1039/D6QM00340K

- The data supporting this article have been included as part of the Supplementary Information.